Journal of Thermal Analysis and Calorimetry, Vol. 75 (2004) 197–204

USE OF DTA-TG IN THE EVALUATION OF AUTOCLAVED CEMENT-BASED SYSTEMS Part I. Cement-brick waste blends

D. S. Klimesch[*]*, M. Gutovic and A. Ray*

University of Technology, Sydney, P.O. Box 123, Broadway, Sydney, NSW 2007, Australia

(Received June 25, 2003; in revised form September 11, 2003)

Abstract

Fired-clay products such as bricks, tiles and pavers, are made in large volumes for use in a variety of construction applications throughout the world. A significant proportion of them ends up being a waste product either during their production process or the demolition of buildings. High pressure steam curing or autoclaving has proven extremely versatile for the manufacture of cement-based building products incorporating waste materials such as fly-ash and blast furnace slag. The nature of hydration products in an autoclaved cement based system incorporating different amounts of finely ground brick waste was investigated by means of thermal analysis and XRD, and is the subject of this paper.

Keywords: autoclaving, brick waste, C–S–H, hydrogarnet, 1.1 nm tobermorite

Introduction

Differential thermal analysis (DTA) has proven an invaluable tool for evaluating the nature of hydration products formed in cement-based systems, particularly those treated hydrothermally [1–5]. Kalousek, who was amongst the first researchers to study phase developments in hydrothermally treated or autoclaved lime–silica [4] and cement–silica [5] systems successfully employed thermal analysis techniques. Currently there is considerable interest in utilising a variety of waste materials such as: newsprint recycling residue [6], timber waste [7], dealuminated kaolin [8] and brick waste [9–11], by incorporating them in building products. The worldwide expansion in the usage and production of autoclaved building materials has created the opportunity for replacing quartz sand and cement (partly or wholly) by these waste materials. Previous work by the present authors [12, 13] has shown that the formation of 1.1 nm tobermorite, the principal binder of most autoclaved calcium silicate based building materials, is enhanced by the addition of finely ground brick waste to blends of Portland cement and quartz sand. To gain better insight into the behaviour of brick waste under autoclaving conditions, blends of Portland cement with different amounts of finely ground brick

* Author for correspondence: E-mail: daniesk@eng.uts.edu.au

1388–6150/2004/ $ 20.00

Akadémiai Kiadó, Budapest
Kluwer Academic Publishers, Dordrecht

waste were prepared and phase developments were evaluated by means of thermal analysis and XRD.

Experimental

The following raw materials were used:

a) Goliath cement (OPC) containing SiO_2 20.0%, CaO 64.2%, Al_2O_3 4.5%, Fe_2O_3 3.7%, SO_3 3.5%, and having a fineness index (Blaine) of 350 m^2 kg^{-1} was produced by Australian Cement, Auburn, NSW, Australia.

b) Crushed brick waste less than 2.38 mm, was derived from a major clay-brick manufacturer in Sydney, Australia. The method of grinding used to produce ground brick fines having a surface area comparable to that of the quartz sand was dry ball milling. Table 1 depicts the major oxides of the brick fines as determined by X-ray fluorescence. The mineralogical composition was determined qualitatively using X-ray powder diffractometry (XRD) using JCPDS powder patterns. The major crystalline phases, in decreasing order of abundance were: quartz, mullite, cristobalite and hematite.

Table 1 Major oxides of brick fines used in this investigation

Major oxides	%
SiO_2	69.7
Al_2O_3	18.6
Fe_2O_3	7.5
K_2O	1.88
MgO	0.95
Na_2O	0.44
CaO	0.20

OPC-brick fines mixtures were prepared using a water-to-total solids ratio of 0.36 as this yielded comparable workability for all the mixtures. Brick fines were added at 0, 10, 20, 30, 40, 50, 60, 70, 80 and 90 mass% as cement replacement. The chemical compositions of the pastes studied are presented in Table 2. Mechanical mixing was conducted in accordance with ASTM C 305 082. Pastes were cast into stainless steel moulds and consolidated on a vibratory table, followed by a 24 h curing period in a moist cabinet. Demoulded specimens were autoclaved for 8 h, 6 h of which were at 180°C under saturated steam. After autoclaving, samples were oven dried at around 105ºC overnight followed by disc milling. Thermal analysis was carried out on powdered samples using a TA-instruments SDT 2960 simultaneous DTA-TG analyser at a heating rate of 10°C min^{-1} under flowing air (20 mL min^{-1}) from 20 to 1000°C. Sample sizes were between 30 to 50 mg and were packed into a Pt–Rh crucible with 20 taps. All DTA-TG curves were evaluated using the TA instruments data analysis software as detailed by Klimesch and Ray [14]. The second de-

rivative differential thermal curves (DDT) were used for peak temperature determinations [15]. X-ray diffraction (XRD) analyses were conducted on powdered specimens using a Siemens D5000 diffractometer and copper $K_{\alpha 1}$ radiation from 3 to 60º 2θ at 0.02° 2θ s^{-1}. XRD patterns were $K_{\alpha 2}$ stripped and corrected for instrumental drift. Crystalline phases were identified using JCPDS powder patterns. Additionally, an X-ray line profile fitting program was used to determine integrated peak heights and areas as well as peak positions of major crystalline phases present.

Table 2 Chemical compositions of pastes studied

Brick fines/ mass%	Cement:brick fines ratio	Bulk mole Ca/Si	Bulk mole Ca/(Al+Si)	Bulk mole Al/(Al+Si)
0	–	3.44	2.72	0.21
10	9.00	2.48	1.94	0.22
20	4.00	1.84	1.43	0.22
30	2.33	1.38	1.07	0.23
40	1.50	1.04	0.80	0.23
50	1.00	0.77	0.59	0.23
60	0.67	0.55	0.42	0.24
70	0.43	0.38	0.29	0.24
80	0.25	0.23	0.18	0.24
90	0.11	0.11	0.08	0.24

Results and discussion

Differential thermal (DT) curves of autoclaved specimens are depicted in Fig. 1. In the following discussion the main observed endotherms (endo) and exotherms (exo) are ascribed to:

ca. 105 to 260°C (endo) not shown	presence of calcium silicate hydrates (C–S–Hs) including 1.1 nm tobermorite (Tob, $C_5S_6H_5$);
ca. 260 to 350°C (endo) not shown	presence of a member of the hydrogarnet (Hyd) series, $C_3AS_{3-x}H_{2x}$, x=0 to 3;
ca. 400 to 500°C (endo)	presence of portlandite (CH);
ca. 500 to 550°C (endo)	presence of α-dicalcium silicate hydrate (α-C_2SH);
ca. 573°C (endo)	crystalline inversion due to unreacted quartz (Q);
ca. 600 to 700°C (endo)	decarbonation of calcium carbonate ($CaCO_3$);
ca. 850 to 900°C (exo)	crystallization of beta-wollastonite (β-CS) from C–S–Hs including ($C_5S_6H_5$).

Table 3 provides a summary of the phases identified by XRD and DTA (Fig. 1). In relation to Table 3, the following points are noteworthy:

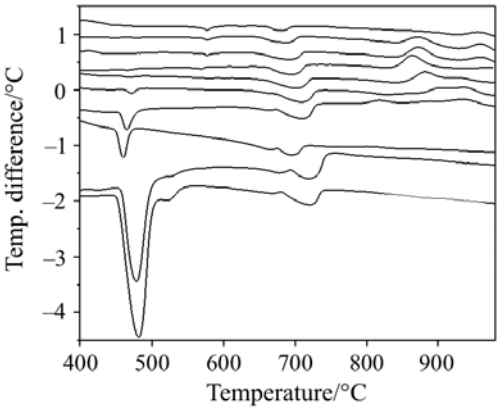

Fig. 1 DT curves of autoclaved specimens made with 0, 10, 20, 30, 40, 50, 60, 70, 80, and 90 mass% brick fines (bottom to top)

(i) Tobermorite was considered absent when the diffraction line due to the (002) peak at around 1.1 nm was not discernible. It is known that this peak is affected in height by the degree of order parallel to the *c*-direction, and that both absolute and relative intensities of peaks in the tobermorite pattern vary with the Ca/Si ratio and the degree of Al-substitution [16, 17].

(ii) C–S–H with main *d*-spacings at around 0.304 and 0.73 nm, referred to as 'fibrous C–S–H' by Kalousek [4], was present in all samples. The XRD peak in the 0.300 nm region due to $CaCO_3$ (Fig. 1 and Table 3) interferes with reflections attributable to C–S–H.

The crystallinity of tobermorite was determined from XRD data by the peak intensity ratio of the 0.308 and 1.1 nm ($H_{0.308}/H_{1.1}$) reflections [18]. In this context, the higher this ratio the less crystalline the material. The variations in the integrated area (arbitrary units) of the 1.1 nm peak and the ratio of peak heights of the 0.308 and 1.1 nm peaks are depicted in Fig. 2. The variation in the observed exotherm temperatures with increasing brick fines addition is shown in Fig. 3.

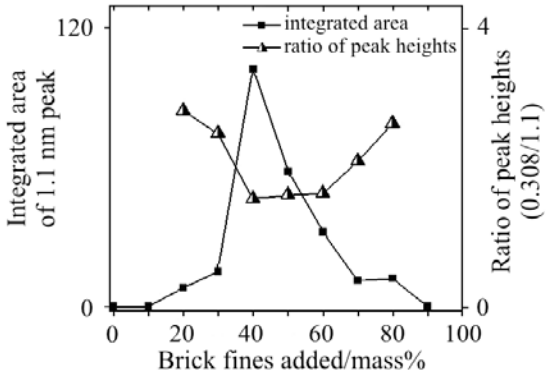

Fig. 2 Showing the variations in the integrated area (arbitrary units) of the 1.1 nm peak and the ratio of peak heights of the 0.308 and 1.1 nm peaks *vs.* brick fines content

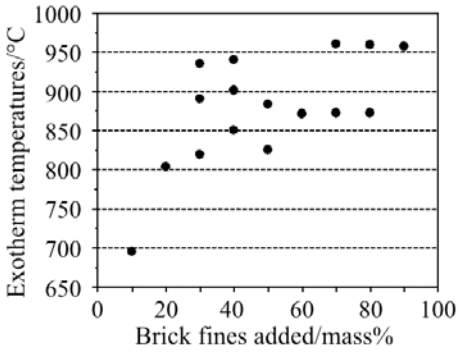

Fig. 3 Showing the variation in the observed exotherm temperatures with increasing brick fines addition

Figures 4 and 5 show the variations in the integrated areas of the 0.304 nm (Fig. 4) and 0.505 nm (Fig. 5) peaks attributable to C–S–H and hydrogarnet, respectively. Also included in these figures are the mass losses from 105 to 260°C and from 260 to 350°C attributable to C–S–H and hydrogarnet, respectively. The authors would like to point out that the mass loss attributable to hydrogarnet is subject to overlap due to the concurrent dehydration reactions of C–S–Hs and tobermorite [19]. Additionally, it is well known that the mass loss due to C–S–Hs and tobermorite varies with Ca/Si ratio and Al content [19, 20].

Table 3 Phases identified by XRD and DTA

Brick fines/mass%	C–S–Hs	Tob*	Hyd	CH	α-C_2SH	$CaCO_3$	Q
0	✓	X	✓	✓	✓	✓	X
10	✓	X	✓	✓	✓	✓	✓
20	✓	✓	✓	✓	X	✓	✓
30	✓	✓	✓	✓	X	✓	✓
40	✓	✓	✓	✓	X	✓	✓
50	✓	✓	✓	X	X	✓	✓
60	✓	✓	✓	X	X	✓	✓
70	✓	✓	✓	X	X	✓	✓
80	✓	✓	X	X	X	✓	✓
90	✓	X	X	X	X	✓	✓

*see text for discussion

In view of the previous comments, the results indicate the following:
1) From Fig. 1 it is evident that the addition of 10% brick fines greatly diminished the formation of α-C_2SH. This phase is relatively dense and is known to reduce the compressive strength in autoclaved products [21].

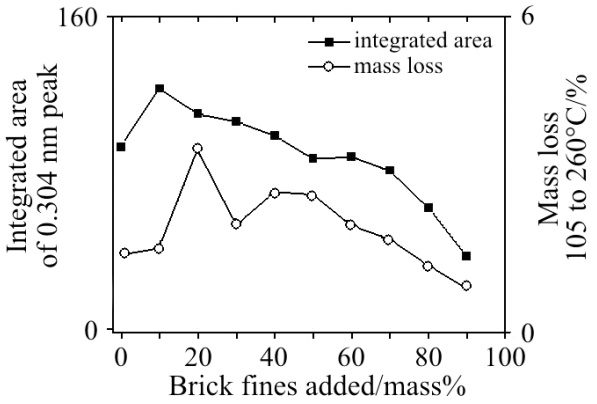

Fig. 4 Variations in the integrated areas of the 0.304 nm peak and mass loss data between 105 and 260°C attributable to C–S–H with increasing brick fines addition

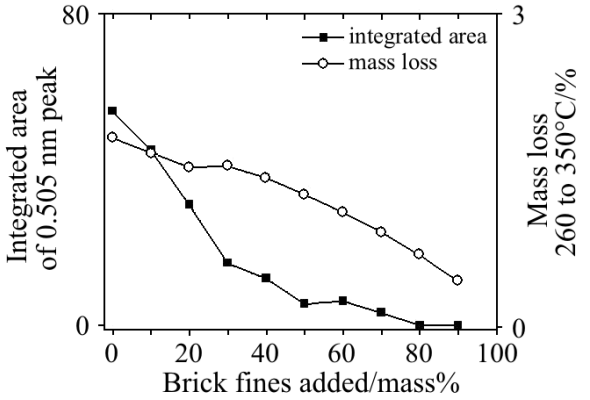

Fig. 5 Variations in the integrated areas of the 0.505 nm peak and mass loss data between 260 and 350°C attributable to hydrogarnet (where present) with increasing brick fines addition

2) From XRD data, the presence of Al-bearing tobermorite (Al-tobermorite) was manifested by the position of the (002) peak, the *d*-spacing ranging from 1.13 to 1.14 nm. Figure 2 shows that additions of 20 and 30% of brick fines promoted the formation of poorly crystalline Al-tobermorite. Additions of 40 to 60% promoted the formation of highly crystalline Al-tobermorite, the amount reaching a maximum at 40% followed by a steady decrease at 50 and 60%. For additions greater than 60%, Al-tobermorite amount and its crystallinity decreased significantly. The variations in Al-tobermorite amount can be explained, at least in part, in terms of the decreasing bulk Ca/Si and Ca/(Al+Si) molar ratios (Table 2). In other words, with decreasing cement:brick fines ratio (Table 2), the availability of CaO from cement decreases resulting in the formation of fewer hydration products.

3) Overall, results from thermal analyses were corroborated by XRD data with the following exception: the variations in the exotherm profiles (Fig. 1) above 800°C, their abundance and associated temperatures (Fig. 3) suggests that additions of 20 and 30%

of brick fines as well as additions greater than 60% of brick fines promoted the formation of poorly crystalline Al-bearing C–S–H [(Al)–C–S–H] rather than Al-tobermorite. A detailed account of the exotherm profiles in relation to C–S–H and tobermorite, with and without Al, may be found elsewhere [15, 22, 23]. Furthermore, interpretations of thermal data can be difficult as there exists the possibility of interactions amongst the mineral phases present in the sample during the thermal experiment including: the formation of new phases from interactions between CaO, through the decomposition of CH, unreacted starting materials and possibly also C–S–Hs [15]; and, solid-state reactions amongst the thermally transformed hydration products and unreacted starting materials [24]. In view of the latter phenomenon, the exotherms at around 950°C (Figs 1 and 3) are believed to be attributable, at least in part, to solid-state reactions amongst the thermally transformed hydration products and unreacted starting materials.

4) The formation of 'fibrous C–S–H' diminished slightly and then appreciably for brick fines additions of 20 to 50% and greater than 60%, respectively (Fig. 4). Concurrently, the amount of hydrogarnet decreased monotonically for brick fines additions of 30 to 70%. Again, these results can be explained, at least in part, in terms of the decreasing bulk Ca/Si and Ca/(Al+Si) molar ratios (Table 2). It may be noted that the total bulk composition, i.e. total bulk Ca/Si and Ca/(Al+Si) molar ratios, does not equal the total reacted composition, since unreacted brick fines remained in all the specimens. More specifically the amount of unreacted material, as determined by the acid-insoluble residue (AIR), ranged from 2.7 to 75.1% for 10 and 90% brick fines additions, respectively. We are currently evaluating the AIR of all specimens and will report the results in future publications.

Conclusions

From the data reported in this paper and within the limits of the experimental conditions chosen for the present work the following conclusions are drawn:

1) The use of waste brick fines in combination with OPC for the production of hydrothermally cured calcium silicate based materials is a viable option for the future.

2) Additions of 40 to 60% of brick fines promoted the formation of highly crystalline Al-tobermorite, the amount reaching a maximum at 40% followed by a steady decrease at 50 and 60%. In contrast, additions of 20 and 30% of brick fines as well as additions greater than 60% of brick fines promoted the formation of poorly crystalline (Al)–C–S–H rather than Al-tobermorite.

3) A combination of thermal analysis and XRD manifested the presence of Al–(C–S–H) and Al-tobermorite more definitively than either technique on its own.

* * *

The authors acknowledge the Australian Research Council for supporting this research via grant DP 0211950.

References

1 G. Mi, F. Saito and M. Hanada, Powder Technology, 93 (1997) 77.
2 X. Huang, D. Jiang and S. Tan, Materials Research Bulletin, 37 (2002) 1885.
3 J. Paya, J. Monzo, M.V. Borrachero, S. Velazquez and M. Bonilla, Cem. Concr. Res., 33 (2003) 1085.
4 G. L. Kalousek, J. Amer. Concr. Inst., 51 (1955) 989.
5 G. L. Kalousek, J. Amer. Concr. Inst., 50 (1954) 365.
6 N. J. Coleman and D. S. Brassington, Materials Research Bulletin, 38 (2003) 485.
7 A. U. Elinwa and Y. A. Mahmood, Cement and Concrete Composites, 24 (2002) 219.
8 N. Y. Mostafa, S. A. S. El-Hemaly, E. I. Al-Wakeel, S. A. El-Korashy and P. W. Brown, Cem. Concr. Res., 31 (2001) 905.
9 M. O'Farrell, S. Wild and B. B. Sabir, Cement and Concrete Composites, 23 (2001) 81.
10 M. O'Farrell, S. Wild and B. B. Sabir, Cem. Concr. Res., 29 (1999) 1781.
11 H. M. L. Schuur, J. Materials in Civil Engineering, November (2000) 282.
12 D. S. Klimesch and A. Ray, in: Proceedings of the International Conference on Composites in Construction, Figueiras et al. (Eds), Porto 2001, p. 47.
13 D. S. Klimesch and A. Ray, Thermochim. Acta, 389 (2002) 195.
14 D. S. Klimesch and A. Ray, Thermochim. Acta, 289 (1996) 41.
15 D. S. Klimesch and A. Ray, J. Therm. Anal. Cal., 70 (2002) 995.
16 J. R. L. Dyczek and H. F. W. Taylor, Cem. Concr. Res., 1 (1971) 589.
17 G. L. Kalousek, J. Amer. Ceram. Soc., 40 (1957) 74.
18 B. Sun and E. Su, Guisuanyan Xuebao, 12 (1984) 281.
19 T. Mitsuda, S. Kobayakawa and H. Toraya, 8th Proc. Int. Congr. Chem. Cem., 3 (1986) 173.
20 H. Hara and N. Inoue, Proc. 1st Int. Symp. Hydrothermal Reactions, (1982) 849.
21 H. F. W. Taylor, Cement Chemistry, 2nd Ed., Thomas Telford, London 1997, p. 342.
22 D. S. Klimesch and A. Ray, Thermochim. Acta, 334 (1999) 115.
23 D. S. Klimesch and A. Ray, J. Therm. Anal. Cal., 56 (1999) 27.
24 M. A. Serry, H. El-Didamony and A. A. Abd El-Kader, Silicates Industriels, 5 (1987) 83.